European Journal of Mechanics B/Fluids 29 (2010) 53–60

Contents lists available at ScienceDirect

European Journal of Mechanics B/Fluids

journal homepage: www.elsevier.com/locate/ejmflu

Optimal control of cylinder wake flow by electro-magnetic force based on adjoint flow field

Hui Zhang, Bao-chun Fan*, Zhi-hua Chen

State Key Laboratory of Transient Physics, Nanjing University of Science and Technology, Nanjing 210094, China

ARTICLE INFO

Article history:
Received 17 January 2008
Received in revised form
28 September 2009
Accepted 1 October 2009
Available online 8 October 2009

Keywords:
Optimal control
Enstrophy
Cylinder wake flow
Electro-magnetic force
Flow control

ABSTRACT

A nonlinear adjoint-based optimal control approach of cylinder wake flow by using electro-magnetic forcing has been proposed and investigated numerically in the paper. A cost functional representing the balance between the enstrophy Ω^2 and the interaction parameter N has been developed, and its corresponding adjoint equations have been derived. The sensitivity of the cost functional is found to be a simple function of the adjoint stream function in the adjoint field. Under the action of optimal force, $N(t)$, the flow separation is suppressed successfully, the oscillations of drag and lift disappear and the total drag coefficient decreases dramatically. Furthermore, the global enstrophy is proved to be equal to the total squared strain during the control, which validates the conservation rule of Okubo-Weiss function.

1. Introduction

The evolution of a turbulent flow is characterized by a vortex cascade, in which large vortices break into small ones accompanied by a direct energy transfer. However, for a two-dimensional laminar flow past a bluff body, the small vortices generated from the body surface will merge into larger vortices, and then develop into a vortex street. The emergence of vortical structures during the flow evolution has led to efforts to characterize regions dominated by the presence of vortices [1]. One of these criteria is the Okubo-Weiss function [2,3], q, defined as the difference between the total squared strain and enstrophy, which provides a simple way to characterize the different regions of the flow field and to identify vortical structures. If $q < 0$ then rotational effects are dominant and if $q > 0$ straining is the dominant process. It is obvious that strong negative values of q are found at the core of vortices, while strong positive values of q occur on the regions surrounding the vortices. It has been shown that the global enstrophy is always equal to the total squared strain field with no-slip boundary conditions [4].

As we know, the viscous flow past a free bluff body may induce undesirable flow separations and vibrations of the body, accompanied by a large fluctuation of drag and lift forces, and acoustic noise. The above phenomena can be suppressed by applying modern flow control methods and technologies. Usually, flow control involves passive and active methods. For passive control, the flow is modified without external energy input [5,6]. In contrast, energy requires to be injected into the flow for active control. Recently, active control methods have attracted more attention, e.g. rotary oscillation control of a cylinder wake [7], sound wave disturbing [8], suction and blowing [9], thermal effect [10] and so on. The Lorentz force was employed to control cylinder wake flow successfully in the 60s of last century, and this type of forcing has attracted new attention in last few years due to its potential applications in engineering situations [11–20].

On the other hand, it is also very important, for the active flow control, to reduce the input energy as small as possible to achieve the goal, which leads to the use of the optimal control theory. The purpose of optimal flow control is to find a control input which makes the cost function minimum under the constraint of N-S equations. It may be classified into two main types: linear and nonlinear optimal control. The linear optimal control relies on the linearized N-S equations, and the classical control theory can be applied straightforwardly [21]. However, the nonlinear optimization is applied to the fully nonlinear N-S equations which may provide perhaps the most rigorous theoretical framework for flow control. One of such methods is the adjoint-based optimization [22,23], which requires to define an adjoint field properly and to obtain the sensitivity of the cost functional by solving the N-S equations and their adjoint equations iteratively. Unfortunately, there is no general approach to deduce the adjoint equations so far.

* Corresponding author.
E-mail address: bcfan@mail.njust.edu.cn (B.-c. Fan).

0997-7546/$ – see front matter © 2009 Elsevier Masson SAS. All rights reserved.
doi:10.1016/j.euromechflu.2009.10.001

In the present paper, we aim at controlling the cylinder wake by suppressing the vortex shedding, which is achieved through the use of the adjoint-based optimal method. A cost functional representing the balance of the enstrophy Ω^2 and the interaction parameter N has been developed, where Ω^2 is taken as the target of regulation and the Lorentz force (the interaction parameter N) is employed as the control input. Based on the cost functional and N-S equations, the corresponding adjoint equations have been derived and the sensitivity of the cost functional is found to be a simple function of the adjoint stream function in the adjoint field.

The optimal control of a cylinder wake flow by electro-magnetic forces based on the adjoint flow field is investigated numerically. The problems considered here are solved with the same method as mentioned in Ref. [24]. The variations of the optimal interaction parameter N with time are described based on the calculations. The evolutions of the flow field, drag and lift coefficients in the control process are also discussed. Moreover, it is validated that, for incompressible two-dimensional flow at low Reynolds number, the global enstrophy is equal to the total squared strain field with the no-slip boundary conditions, which does not dependent on the boundary shape and the existence of body forces or chemical reactions in the flow field.

2. Lorentz force control of cylinder wake

For the control of a circular cylinder wake in an electrically low-conducting fluid, the cylinder surface consists of two half cylinders mounted with alternating streamwise electrodes and magnets as shown in Fig. 1. In this way, the Lorentz force is directed parallel to the cylinder surface and decays exponentially in the radial direction, which can be described by a distributed function given by Weier et al. [12]

$$|F_\theta| = e^{-\alpha(r-1)} \tag{1}$$

$$F_r = 0$$

where r and θ are polar coordinates, $\boldsymbol{F}$ is the distribution function of dimensionless Lorentz force, subscripts r and θ represent the components in r and θ directions, respectively. α is a constant, representing the effective depth of Lorentz force in the fluid.

Introducing exponential-polar coordinates system (ξ,η), where $r = e^{2\pi\xi}$ and $\theta = 2\pi\eta$, the governing equations describing such fluid-structure problem can be written in the dimensionless form

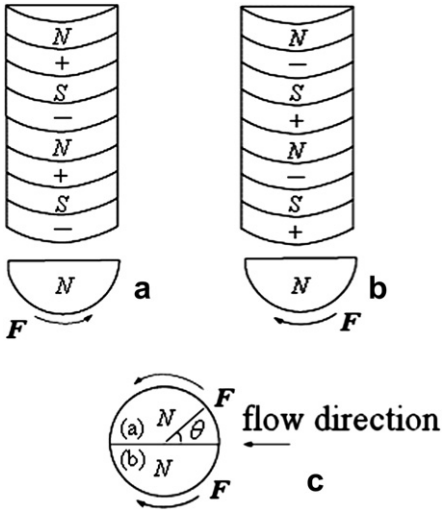

Fig. 1. Lorentz force on the cylinder surface.

$$\mathcal{N}(\mathbf{q})\mathbf{q} = \begin{pmatrix} -H\Omega \\ N\mathbb{F}(\xi) \end{pmatrix} \tag{2}$$

where the flow state $\mathbf{q} = \begin{pmatrix} \Omega \\ \psi \end{pmatrix}$, $\mathcal{N}(\mathbf{q})$ is the Navier–Stokes operator in the exponential-polar coordinates,

$$\mathcal{N}(\mathbf{q})\mathbf{q} = \begin{pmatrix} \dfrac{\partial^2\psi}{\partial\xi^2} + \dfrac{\partial^2\psi}{\partial\eta^2} \\ H\dfrac{\partial\Omega}{\partial t} + \dfrac{\partial(U_r\Omega)}{\partial\xi} + \dfrac{\partial(U_\theta\Omega)}{\partial\eta} - \dfrac{2}{\mathrm{Re}}\left[\dfrac{\partial^2\Omega}{\partial\xi^2} + \dfrac{\partial^2\Omega}{\partial\eta^2}\right] \end{pmatrix}$$

and $\mathbb{F}(\xi) = H^{\frac{1}{2}}\left[\dfrac{\partial F_\theta}{\partial\xi} + 2\pi F_\theta\right]$

where the stream function ψ is defined as $\partial\psi/\partial\eta = U_r = H^{1/2}u_r$, $-(\partial\psi/\partial\xi) = U_\theta = H^{1/2}u_\theta$, while the vorticity Ω is defined as $\Omega = (1/H)((\partial U_\theta/\partial\xi) - (\partial U_r/\partial\eta))$, with u_r and u_θ the velocity components in r and θ directions, respectively. Furthermore $H = 4\pi^2 e^{4\pi\xi}$, $\mathrm{Re} = 2u_\infty a/\nu$, u_∞ is the free-stream velocity, ν is the kinematic viscosity, a is the cylinder radius, the non-dimensional time is $t = t^* u_\infty/a$. The interaction parameter is defined as $N = j_0 B_0 a/\rho u_\infty^2$, with the current density $j_0 = \sigma E_0$, σ the electric conductivity, E_0 the electric field and B_0 the magnetic field.

The flow is considered to be potential initially and therefore

$$\text{at } t = 0,\ \psi = 0,\ \Omega = -\frac{1}{H}\frac{\partial^2\psi}{\partial\xi^2} \qquad \text{on } \xi = 0$$

$$\psi = -2sh(2\pi\xi)\sin(2\pi\eta),\ \ \Omega = 0, \quad \text{on } \xi > 0$$

$$\text{at } t > 0,\ \psi = 0,\ \Omega = -\frac{1}{H}\frac{\partial^2\psi}{\partial\xi^2} \qquad \text{on } \xi = 0$$

$$\psi = -2sh(2\pi\xi)\sin(2\pi\eta),\ \Omega = 0 \quad \text{on } \xi = \xi_\infty$$

The calculations have been performed numerically. The equation of vorticity transport is solved by using the Alternative-Direction Implicit (ADI) algorithm, and the equation of stream function is integrated by means of a Fast Fourier Transform (FFT) algorithm. More details can be found in Ref. 19. Numerical results in the paper are obtained at $\mathrm{Re} = 150$with the computational step size $\Delta\xi = 0.004$, $\Delta\eta = 0.002$ and $\Delta t = 0.005$.

3. Okubo-Weiss function and conservation rule

By defining the two-dimensional divergence operator $\nabla = (\partial_1\partial_2)^T$, the gradient of the velocity $\mathbf{u}$ can be written as

$$\nabla\mathbf{u} = \begin{pmatrix} \partial_1 u_1 & \partial_2 u_1 \\ \partial_1 u_2 & \partial_2 u_2 \end{pmatrix} \tag{3}$$

and

$$\nabla\mathbf{u}\cdot\mathbf{u} = \begin{pmatrix} u_1(\partial_1 u_1) & u_2(\partial_2 u_1) \\ u_1(\partial_1 u_2) & u_2(\partial_2 u_2) \end{pmatrix} \tag{4}$$

For an incompressible flow, $\nabla\cdot\mathbf{u} = \partial_1 u_1 + \partial_2 u_2 = 0$, we have

$$\nabla\cdot((\nabla\mathbf{u})\cdot\mathbf{u}) = -2\det(\nabla\mathbf{u}) = \frac{1}{2}q \tag{5}$$

where $q = S_1^2 + S_2^2 - \Omega^2$ is called the Okubo-Weiss function [3], $S_1 = \partial_1 u_1 - \partial_2 u_2$ and $S_2 = \partial_2 u_1 - \partial_1 u_2$ are the strain denoting the compression along the normal direction and the deformation along the tangent direction, respectively. $\Omega = \partial_1 u_2 - \partial_2 u_1$ is the vorticity, and Ω^2 is the enstrophy.

For a viscous flow around a body, $\mathbf{u} = 0$ on the body surface C, and $\nabla\mathbf{u} = 0$on the infinite undisturbed boundary, then equation (4) becomes

$$\iint_S \nabla\cdot((\nabla\mathbf{u})\cdot\mathbf{u})\mathrm{d}A = \oint_C (\nabla\mathbf{u})\cdot\mathbf{u}\cdot\mathbf{n}\mathrm{d}l = 0$$

where $\mathbf{n}$ is the normal vector on the body surface, then

$$\iint_S q\mathrm{d}A = Q = 0 \tag{6}$$

or

$$\iint_S \Omega^2\mathrm{d}A = \iint_S \left(S_1^2 + S_2^2\right)\mathrm{d}A \tag{7}$$

which indicates that the integral value of the Okubo-Weiss function q over the whole flow field is equal to zero, or the global enstrophy is equal to the total squared strain field [25], even if Lorentz forces exist in the flow field.

4. Cost functional

Due to the increase of momentum in the boundary under the action of streamwise Lorentz forces, flow separation around a circular cylinder can be suppressed. Since the flow separation causes vortex shedding, force fluctuations, acoustic noise and so on. Therefore, separation control is potentially important for certain engineering flow configurations.

The purpose of optimal flow control is to determine the right control input that effectively tailors the flow. Hence, the control input should vary with the transient flow field and depends on the state variables of the flow field. The key element of an optimal flow control is the minimization of a cost functional. Therefore, the cost functional should contain three kinds of important physical variables i.e. the control input, the state variables of the flow field and the price of the control.

In the present work, control of electrically low-conducting fluids by Lorentz forces is considered and therefore, the interaction parameter N, a dimensionless magnitude of Lorentz force, is taken as a control input. As mentioned in Ref. [26], the state variable, a quantity of physical interest regulated or minimized in control such as the enstrophy Ω^2, the skin-friction drag $\Omega\sin(2\pi\eta)$, $\Omega\cos(2\pi\eta)$ and the skin-pressure drag $\partial\Omega/\partial\xi\sin(2\pi\eta)$ etc. can be chosen optionally. Several cases of physical interest may be represented by a cost functional of the following generic form

$$\mathcal{J}(N) = -\frac{Hd_1}{2}\int_0^T\iint_\Sigma \Omega^2\mathrm{d}v\mathrm{d}t - \frac{2d_2}{R_e}\int_0^T\int_0^1 \Omega K_1\mathrm{d}\eta\mathrm{d}t - \frac{2d_3}{R_e}\int_0^T\int_0^1 \Omega K_2\mathrm{d}\eta\mathrm{d}t$$
$$-\frac{2d_4}{R_e}\int_0^T\int_0^1 \frac{\partial\Omega}{\partial\xi}K_1\mathrm{d}\eta\mathrm{d}t - \frac{2d_5}{R_e}\int_0^T\int_0^1 \frac{\partial\Omega}{\partial\xi}K_2\mathrm{d}\eta\mathrm{d}t + \frac{l^2}{2}\int_0^T\int_0^1 N^2\mathrm{d}\eta\mathrm{d}t \tag{8}$$

where $K_1 = \sin(2\pi\eta)$, $K_2 = \cos(2\pi\eta)$. l^2 is a weighting factor representing the price of the control. If the control is 'low cost', its value is small, and vice versa. The constants d_i account for the relative weight of each individual term and $\sum d_i = 1$.

In order to validate the conservation rule[i]of the above Okubo-Weiss function and simplify the optimal problem, we choose the enstrophy as the quantity of physical interest which is directly related to the vortical structures in the flow field. Then, the cost functional can be written as

$$J(N) = -\frac{H}{2}\int_0^T\iint_S \Omega^2\mathrm{d}V\mathrm{d}t + \frac{l^2}{2}\int_0^T\int_0^1 N^2\mathrm{d}\eta\mathrm{d}t \tag{9}$$

Considering a perturbation J' to the cost function resulting from an arbitrary perturbation N', then we have

$$J' = \int_0^T\iint_S \frac{\mathcal{D}J}{\mathcal{D}N}N'\mathrm{d}V\mathrm{d}t = -H\int_0^T\iint_S \Omega\Omega'\mathrm{d}V\mathrm{d}t + l^2\int_0^T\int_0^1 NN'\mathrm{d}\eta\mathrm{d}t \tag{10}$$

where, the prime indicates the Fréchet differential and T is the period for optimizing. Only one properly defined adjoint field is established and the cost functional perturbation J' can be expressed as a simple linear function of the direction of the control perturbation N' through the solution of an adjoint problem which reveals the direction DJ/DN directly.

5. Adjoint flow field

From Eq. (2), the linearized perturbation equations are given by

$$\mathcal{N}'(\mathbf{q})\mathbf{q}' = \begin{pmatrix} -H\Omega' \\ N'\mathbb{F} \end{pmatrix} \tag{11}$$

with initial and boundary conditions

$$\text{at } t = 0,\ \psi' = 0,\ \Omega' = 0,\ \frac{\partial\psi'}{\partial\xi} = 0,\ \frac{\partial\psi'}{\partial\eta} = 0$$

$$\text{at } t > 0, \psi' = 0, \frac{\partial\psi'}{\partial\xi} = -U'_\theta = 0,\ U'_r = 0,\ \xi = 0,$$

$$\psi' = 0,\ \frac{\partial\psi'}{\partial\xi} = 0,\ \Omega' = 0, \frac{\partial\Omega'}{\partial\xi} = 0 \text{ on } \xi = \infty$$

where the flow perturbation state $\mathbf{q}' = \begin{pmatrix}\Omega' \\ \psi'\end{pmatrix}$, $\mathcal{N}'(\mathbf{q})\mathbf{q}'$ is given by

$$\mathcal{N}'(\mathbf{q})\mathbf{q}' = \begin{pmatrix} \dfrac{\partial^2\psi'}{\partial\xi^2} + \dfrac{\partial^2\psi'}{\partial\eta^2} \\ H\dfrac{\partial\Omega'}{\partial t} + \dfrac{\partial(U_r\Omega' + U'_r\Omega)}{\partial\xi} + \dfrac{\partial(U_\theta\Omega' + U'_\theta\Omega)}{\partial\eta} - \dfrac{2}{\mathrm{Re}}\left[\dfrac{\partial^2\Omega'}{\partial\xi^2} + \dfrac{\partial^2\Omega'}{\partial\eta^2}\right] \end{pmatrix}$$

Once the cost functional J is defined mathematically, a properly defined adjoint field has to be derived to determine the gradient of the cost functional [24]. Here the adjoint flow field is governed by

$$\mathcal{N}'(\mathbf{q})^*\mathbf{q}^* = \begin{pmatrix} -H\left(\Omega^* - \Omega\right) \\ 0 \end{pmatrix} \tag{12}$$

with initial and boundary conditions

$$\text{at } t = T,\ \psi^* = 0,\ \Omega^* = 0$$

$$\text{at } t < T,\ \psi^* = 0,\ \Omega^* = -\frac{1}{H}\frac{\partial^2\psi^*}{\partial\xi^2}, \text{on } \xi = 0$$

$$\psi^* = 0, \Omega^* = 0, \text{on } \xi = \infty$$

where the adjoint state $\mathbf{q}^* = \begin{pmatrix} \Omega^* \\ \psi^* \end{pmatrix}$, $\mathcal{N}'(\mathbf{q})^*\mathbf{q}^*$ is given by

$$\mathcal{N}'(\mathbf{q})^*\mathbf{q}^* = \begin{pmatrix} -\left(\dfrac{\partial^2\psi^*}{\partial\xi^2} + \dfrac{\partial^2\psi^*}{\partial\eta^2}\right) \\ -\left[H\dfrac{\partial\Omega^*}{\partial t} + \dfrac{\partial\left(U_r\Omega^* + U_r^*\Omega\right)}{\partial\xi} + \dfrac{\partial\left(U_\theta\Omega^* + U_\theta^*\Omega\right)}{\partial\eta} - \dfrac{2}{\mathrm{Re}}\left(\dfrac{\partial^2\Omega^*}{\partial\xi^2} + \dfrac{\partial^2\Omega^*}{\partial\eta^2}\right)\right] \end{pmatrix}$$

Defining $\langle \mathbf{a}, \mathbf{b} \rangle$ as the inner product of vector $\mathbf{a}$ and $\mathbf{b}$ over the domain in space-time, then we obtain

$$\left\langle \mathcal{N}'(\mathbf{q})\mathbf{q}', \mathbf{q}^* \right\rangle = \int_0^T\int_S \begin{pmatrix} -H\Omega' \\ N'\mathbb{F} \end{pmatrix}\begin{pmatrix} \Omega^* \\ \psi^* \end{pmatrix} \mathrm{d}V\mathrm{d}t \tag{13}$$

and

$$\left\langle \mathbf{q}', \mathcal{N}'(\mathbf{q})^*\mathbf{q}^* \right\rangle = \int_0^T\int_S \begin{pmatrix} -H\left(\Omega^* - \Omega\right) \\ 0 \end{pmatrix}\begin{pmatrix} \Omega' \\ \psi' \end{pmatrix} \mathrm{d}V\mathrm{d}t \tag{14}$$

From the integrations by parts, we also get

$$b = \left\langle \mathcal{N}'(\mathbf{q})\mathbf{q}'\mathbf{q}^* \right\rangle = \left\langle \mathcal{N}'(\mathbf{q})\mathbf{q}', \mathbf{q}^* \right\rangle - \left\langle \mathbf{q}', \mathcal{N}'(\mathbf{q})^*\mathbf{q}^* \right\rangle \tag{15}$$

Substituting Eq. (13) and (14) into Eq. (15), we have

$$b = \int_0^T\int_S N'\mathbb{F}\psi^*\,\mathrm{d}v\mathrm{d}t - \int_0^T\int_S H\Omega\Omega'\,\mathrm{d}v\mathrm{d}t \tag{16}$$

then

$$\int_0^T\int_S N'\mathbb{F}\psi^*\,\mathrm{d}v\mathrm{d}t = \int_0^T\int_S H\Omega\Omega'\,\mathrm{d}v\mathrm{d}t \tag{17}$$

As N' is arbitrary, from Eq. (10) we may identify the desired gradient as

$$\frac{\mathcal{D}J}{\mathcal{D}N} = -\int_S \mathbb{F}\psi^*\,\mathrm{d}v + l^2N \tag{18}$$

Therefore, the stream function ψ^* in the adjoint field is a measure of the sensitivity of the cost functional.

6. Optimal control

When the control input $N$and the period of the control time $T$are set, the development of the flow field $\mathbf{q}$ from $t = 0$ to $t = T$ can be obtained by the numerical integration of Eq. (2). Then the development of the adjoint flow field, $\mathbf{q}^*$, can be obtained by the integration of Eq. (12) and marching backward from $t = T$ to $t = 0$. The computation of the adjoint field requires the storage of the flow field $\mathbf{q}$. Finally, $\mathcal{D}J/\mathcal{D}N$ can be calculated from Eq. (18) based on the adjoint field $\mathbf{q}^*$ at $t = 0$.

The purpose of optimal flow control is to determine the optimal control input function $N(t)$, which is achieved through the minimizing cost function, thus

$$\frac{\mathcal{D}J}{\mathcal{D}N} = 0 \tag{19}$$

or

$$\int_S \mathbb{F}\psi^*\,\mathrm{d}v = l^2N \tag{20}$$

With the gradient information described above, a strategy for solving Eq. (19) using an iteration method may be proposed as

$$N^k = N^{k-1} - \beta^k\frac{DJ\left(N^{k-1}\right)}{DN} \tag{21}$$

where k indicates the iteration number and β^k is a parameter of descent which governs the magnitude for update.

The receding-horizon predictive control setting is employed to discuss the optimal control problems as shown in Fig. 2 [24]. When the flow field at $t = T_a$ is determined and the optimization horizon T is set, then according to the predicted N, DJ/DN can be obtained by the forward and backward integrations as described above, and the iteration processes, shown as the dashed lines and dot-dashed lines in the Fig. 2, are performed till $(DJ/DN) = 0$. Once the optimal input N is determined, the flow is advanced by some portion T_a, and the optimization process begins again.

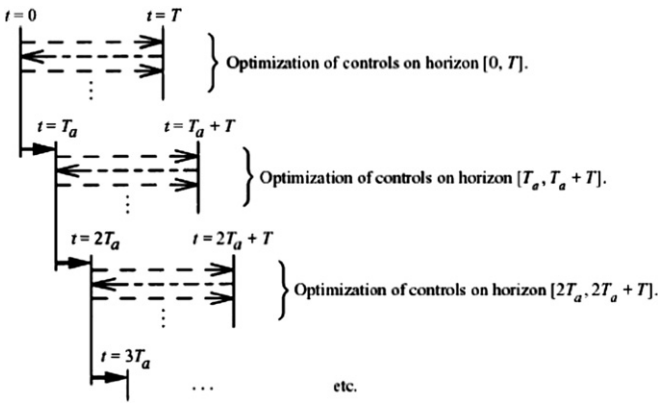

Fig. 2. The sequence of events in receding-horizon predictive control [24].

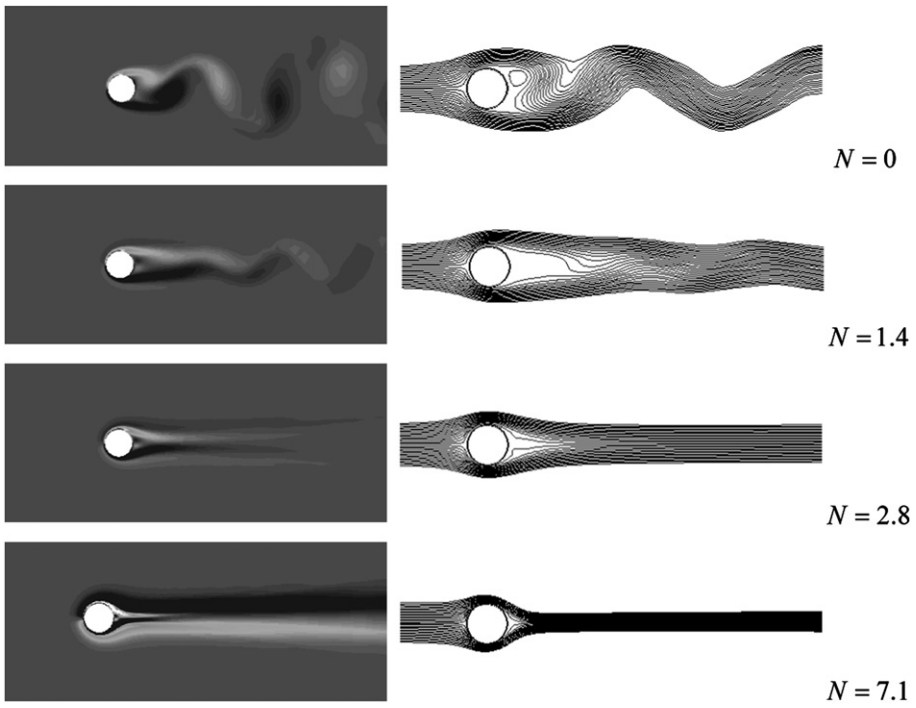

Fig. 3. Instantaneous vorticity contours and steamlines of cylinder wake with open-loop control at $t = 548$.

Formulations of optimizing control over longer time horizons T have a significant advantage over those with shorter time horizons [24]. However, the larger the optimization horizon, the more difficult the optimization problem becomes. It appears that the optimization of the nonlinear Navier–Stokes control problem over an infinite time horizon would require the solution of a very difficult Hamilton-Jacobi-Bellman (HJB) problem in infinite dimensions, and is computationally intractable. In Ref.24, the optimization horizon, $T \geq 25\Delta t$ is considered sufficiently. In this paper, we choose $T = 30\Delta t$, and $T_a = \Delta t$.

7. Results and discussions

7.1. Open-loop control

Fig. 3 shows the computed vorticity contours and streamlines of the cylinder wake controlled by Lorentz forces triggered at $t = 500$, with different interaction parameter values $N = 0$, 1.4, 2.8 and 7.1 at $t = 548$. For $N = 0$, the flow is unsteady and shows the characteristic features of the von Karman vortex street. Although the flow is still unsteady for a small Lorentz force, $N = 1.4$, the flow separation region is greatly diminished and a region with two relatively small recirculating bubbles occurs behind the cylinder. The separation is fully suppressed with the control input $N = 2.8$.With further increase of the interaction parameter, e.g. $N = 7.1$, the fluid is strongly accelerated by the Lorentz force, so that the streamlines become closed to each other.

The dimensionless drag and lift coefficients are defined as

$$C_d = \frac{F_x}{\rho u_\infty^2 a}, C_l = \frac{F_y}{\rho u_\infty^2 a}$$

where F_x and F_y denote the total force components in streamwise and normal direction, respectively. The total drag is composed of two parts, i.e

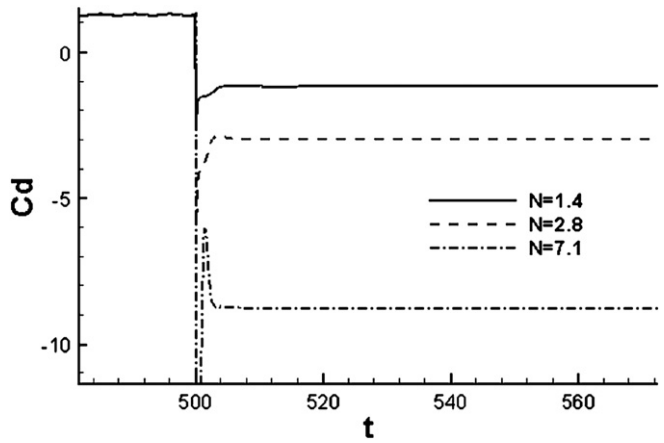

Fig. 4. Variations of drag force coefficient $C_d$with time t for the open-loop control for $N = 1.4$, 2.8 and 7.1.

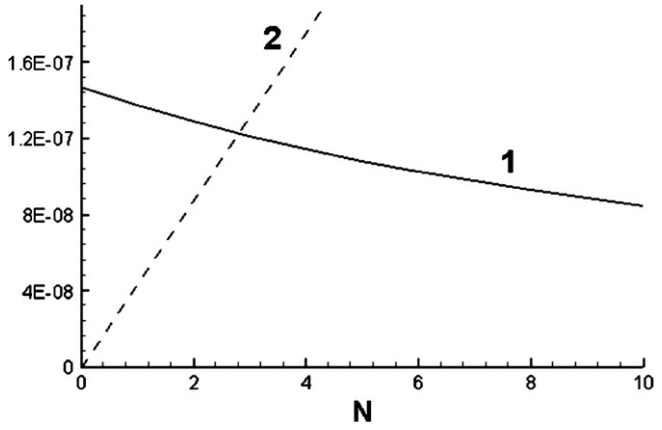

Fig. 5. The optimal $N(t)$ value determined by the intersection point of the solid line 1 (the integral curve related with the adjoint flow) and the dashed line 2 (the line in proportion to N).

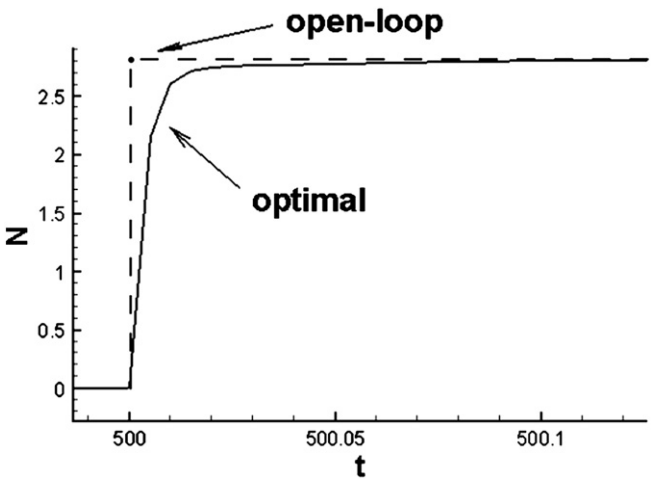

Fig. 6. Variations of optimal actuator $N(t)$ during the optimal control process.

$$F_x = F_{px} + F_{\tau x}$$

where F_{px} and $F_{\tau x}$ denote the pressure drag and the friction drag, respectively. Then, the pressure drag and the friction drag coefficients are given by

$$C_p = \frac{F_{px}}{\rho u_\infty^2 a}, C_f = \frac{F_{\tau x}}{\rho u_\infty^2 a}$$

Fig. 4 shows the time evolution of drag force coefficient C_d under the action of Lorentz forces of different strengths. During the control, the drag coefficient decreases dramatically at the beginning, and finally becomes steady. It is also observed that the amount of drag reduction increases when the interaction parameter N increases.

7.2. Optimal control input

During the optimal control, the control input $N(t)$ varying with the transient flow field is determined by Eq. (20), in which the right side term is in proportion to N and the left side term is related to an integration of ψ^* over the adjoint flow field, which is dependent upon N. Therefore, the optimal $N(t)$ can be determined at the intersection point of the two curves shown in Fig. 5, where the solid line 1 denotes the integral curve related with the adjoint flow, and the dashed line 2 denotes the line in proportion to N.

The quantity l^2 represents the price of the control in Eq. (8) and it is also related implicitly with N_0, a fixed interaction parameter number required for maintaining the final controlled flow field. The time evolution of the optimal $N(t)$ with $l^2 = 4.29^*10^{-8}$, corresponding to $N_0 = 2.8$, is shown as the solid line in Fig. 6. The value of N increases rapidly at the triggering time $t = 500$, and after a short time interval (about $\delta t = 0.2$), it tends to remain constant N_0, and the flow become steady. The dashed line in Fig. 6 represents the variation of N in the open-loop control, where $N = 2.8$ after the electromagnetic actuators are triggered. It is obvious that the solid line lies below the dashed line during the control process, which implies that the energy consumption of optimal control is less than that of open-loop control at the very early stage.

7.3. Variations of force coefficients in optimal control

The time histories of the force coefficients under both the open and optimal control are shown in Fig. 7, where (a), (b), (c) and (d) correspond to the drag C_d, lift C_l, friction drag C_f and pressure drag C_p coefficients, respectively. It has been shown that all the above force coefficients, specially the lift coefficient C_l, oscillate regularly before the control due to the vortex shedding off the cylinder. However, after the control, these fluctuations decrease gradually

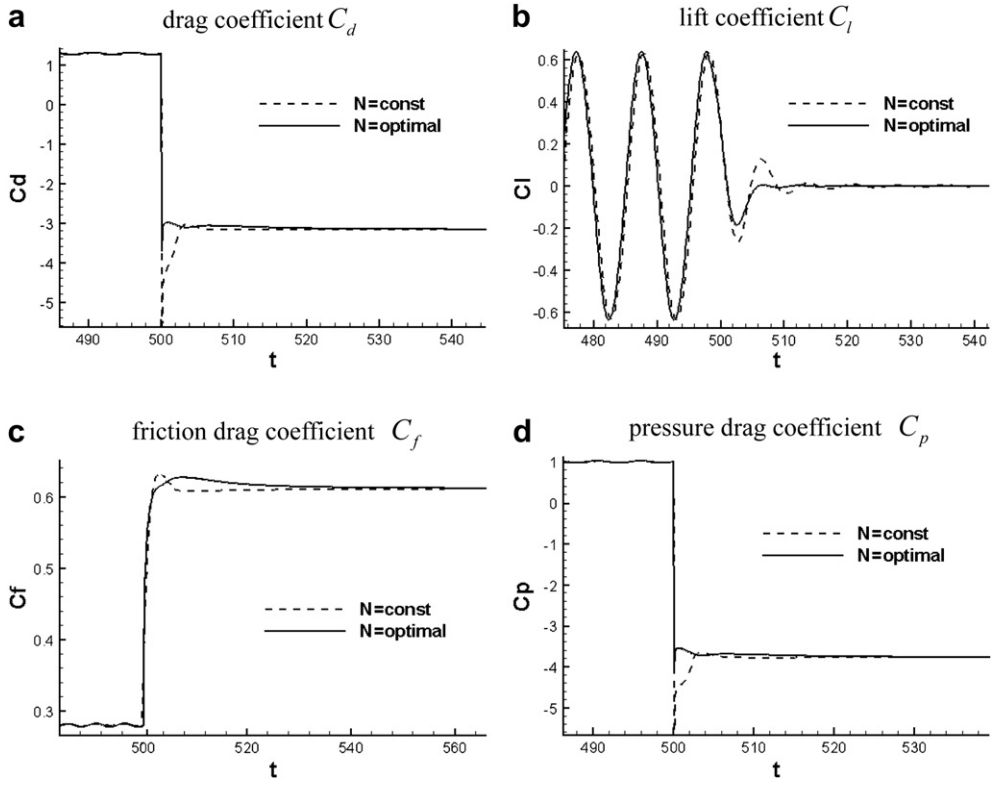

Fig. 7. Time history of force coefficients during the open and optimal control process.

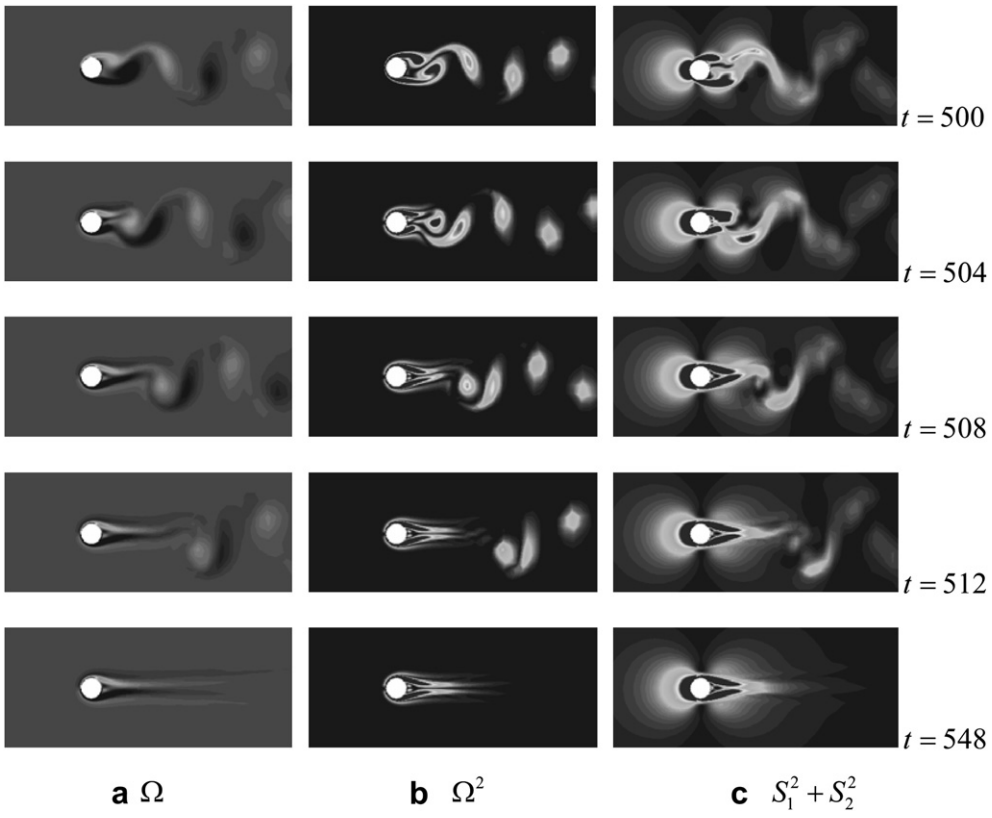

Fig. 8. Variations of vorticity, enstrophy and strain during the control.

since the flow separation and vortex shedding are suppressed at about one single shedding period. The total drag coefficient is composed of the pressure and friction drag coefficients. The increase of vorticity at the wall due to the control leads to a rise of the friction coefficient (Fig. 7c). However, the pressure coefficient decreases after the control, which dominates the variations of the total drag force. Generally, the final effect of the optimal control is almost the same as that of the open-loop control ($N = N_0$), but the optimal control is more effective on the suppression of force fluctuations than the open control at the beginning of the control (Fig. 7a and b), so that the drag and lift forces tend to become steady more quickly under optimal control.

It can be seen from Fig. 7b that the optimal control starts at a time ($t = 500$) when the lift is close to zero. However, our numerical tests indicate that, even at the largest lift moment, the initial variation of optimal Lorentz force is only slightly different, as shown in Fig. 6. Furthermore, when the flow becomes steady, the Lorentz force turns to the same value, 2.8, finally, which has no relation to the triggering time of control for a well-developed flow. In addition, as shown from Fig. 7a, the drag coefficient becomes negative, -3.0, at a very short time after the application of the optimal Lorentz force ($N = 2.8$), which indicates that the Lorentz force creates a net thrust, and modifies the flow field near the cylinder.

7.4. Evolution of the flow field in optimal control

The flow evolutions during control are shown in Fig. 8. The variations of the vorticity field in control are shown in Fig. 8a, where gray denotes positive values and black refers to negative values. The modification of the vorticity field around the cylinder is distinct, and flow separation is suppressed fully at last. The variations of the enstrophy field in the controlled case are shown in Fig. 8b. The enstrophy, being a measure of the vortical motion in the fluid is large at the core of vortices, and small on the edges of the vortices or between vortices. While a vortex moves downstream, under the effects of the enstrophy dissipation the rotation of the core and its shear effect become weak. However, near the surface of the cylinder, the velocity gradient increases due to the action of Lorentz force, and it also leads to an increase of the enstrophy. In Fig. 8c, the gray color denotes small values of the strain describing the deformation of fluid, while the dark color corresponds to high values. The deformation is large on the front and rear stagnation points of the cylinder and also at the core of the vortices shed from the cylinder. On the other hand, the strain is weak far away from the cylinder.

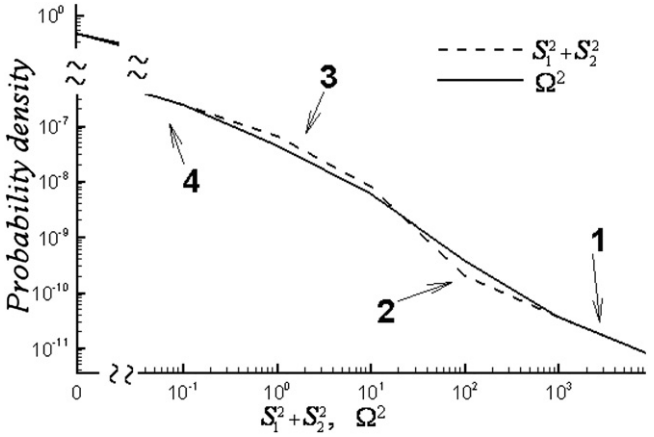

Fig. 9. Probability density distributions of the enstrophy and squared strain in flow field around the cylinder without control.

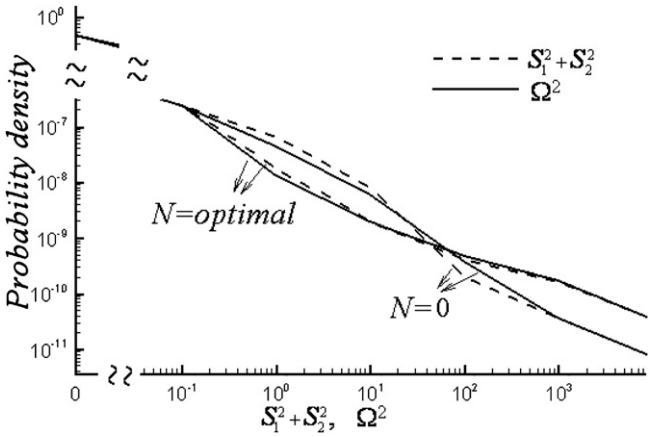

Fig. 10. Probability density distributions of enstrophy and squared strain under optimal control.

7.5. Conservation rule during control

The probability density distributions of enstrophy and squared strain in the flow field without control at $t = 500$ are shown in Fig. 9. Four different regions can be distinguished in this figure. In region 1, distributed mainly near the cylinder surface, enstrophy is almost equal to squared strain and their values are highest. Region 2 is the area dominated by rotation, where the enstrophy is greater than the squared strain and their values are less than that in region 1. In region 3, corresponding to the periphery of vortices, the enstrophy is less than squared strain, and their values are less than that in region 2. Region 4 corresponds to far field from the cylinder, where the enstrophy and squared strain are the least compared to the other three regions. From region 1 to region 4, the values of enstrophy and squared strain decrease sequentially, although the areas that they occupy increase. Despite enstrophy and squared strain are locally different in different regions, the global enstrophy is always equal to the total squared strain field [25], thus the integral of Okubo-Weiss function q in the whole flow region is always equal to zero.

The probability density distributions of enstrophy and squared strain under the optimal control of the Lorentz force are shown in Fig. 10. With the application of streamwise Lorentz force, the velocity gradient increases dramatically near the cylinder surface due to the flow acceleration, which causes the intensity of enstrophy and strain to increase rapidly and the curve of region 1 to rise. The regions 2 and 3 are reduced obviously, since the flow separation on the cylinder surface is suppressed and the vortex street behind the cylinder disappears. Even the distributions of enstrophy and squared strain are changed locally in the control, the global enstrophy remains to be equal to squared strain at all time, which means the integral value of the Okubo-Weiss function over the whole flow field is equal to zero.

8. Conclusion

In this paper, the nonlinear adjoint-based optimal control approach of a cylinder wake flow by electro-magnetic force is investigated numerically. The optimizing force $N(t)$ varying with the transient flow field increases rapidly at the triggered time, and then tends to remain constant. Under the action of $N(t)$, the flow separation is suppressed successfully, which leads to the suppression of drag and lift oscillations. The optimal control is effective on the force fluctuation suppression at the beginning of control, and the global enstrophy is proved to be equal to the total squared strain during the control, which validates the conservation rule of the Okubo-Weiss function.

Acknowledgment

The authors are grateful to Professor Y. Andreopoulos (CCNY) for his help in correcting grammatical errors and improving the written style of this article.

References

[1] A. Provenzale, Transport by coherent barotropic vortices. Annual Review of Fluid Mechanics 31 (1999) 55–93.
[2] A. Okubo, Horizontal dispersion of floatable particles in the vicinity of velocity singularities such as convergences. Deep-Sea Resarch 17 (1970) 45–454.
[3] J. Weiss, The dynamics of enstrophy transfer in two-dimensional hydrodynamics. Physica D 48 (1991) 273–294.
[4] L. Zavala Sansón, J. Sheinbaum, Elementary properties of the enstrophy and strain fields in confined two-dimensional flows. European Journal of Mechanics 27 (2008) 54–61.
[5] K. Kwon, H. Choi, Control of laminar vortex shedding behind a circular cylinder using splitter plates. Physics of Fluids 8 (1996) 479–486.
[6] P.J. Strykowski, K.R. Sreenivasan, On the formation and suppression of vortex 'shedding' at low Reynolds numbers. Journal of Fluid Mechanics 218 (1990) 71–107.
[7] P.T. Tokumaru, P.E. Dimotakis, Rotary oscillation control of a cylinder wake. Journal of Fluid Mechanics 224 (1991) 77–90.
[8] K. Roussopoulos, Feedback control of vortex shedding at low Reynolds numbers. Journal of Fluid Mechanics 248 (1993) 267–296.
[9] Z.J. Li, I.M. Navon, M.Y. Hussaini, F.X. Le Dimet, Optimal control of cylinder wakes via suction and blowing. Computers and Fluids 32 (2003) 149–171.
[10] L.C. Lecordier, L.W.B. Browne, S. Le Masson, F. Dumouchel, P. Paranthoen, Control of vortex shedding by thermal effect at low Reyolds numbers. Experimental Thermal and Fluid Science 21 (2000) 227–237.
[11] A. Gailitis, O. Lielausis, On a possibility to reduce the hydrodynamical resistance of a plate in an electrolyte. Applied Magnetohydrodynamics 12 (1961) 143–146.
[12] T. Weier, G. Gerbeth, G. Mutschke, E. Platacis, O. Lielausis, Experiments on cylinder wake stabilization in an electrolyte solution by means of electromagnetic forces localized on the cylinder surface. Experimental Thermal and Fluid Science 16 (1998) 84–91.
[13] T. Weier, G. Gerbeth, Control of separated flows by time periodic Lorentz forces. European Journal of Mechanics B/Fluid 23 (2004) 835–849.
[14] S.J. Kim, C.M. Lee, Investigation of the flow around a circular cylinder under the influence of an electromagnetic force. Experiments in Fluids 28 (2000) 252–260.
[15] Z.H. Chen, N. Aubry, Active control of cylinder wake. Communications in Nonlinear Science & Numerical Simulation 10 (2005) 205–216.
[16] Z.H. Chen, N. Aubry, Closed-loop control of vortex-induced vibration. Communications in Nonlinear Science & Numerical Simulation 10 (2005) 287–297.
[17] Z.H. Chen, B.C. Fan, N. Aubry, B.M. Zhou, Electro-magnetic control of vortex shedding behind a circular cylinder. Chinese Physics Letters 23 (1) (2006) 154–157.
[18] O. Posdziech, R. Grundmann, Electromagnetic control of seawater flow around circular cylinders. European Journal of Mechanics B/Fluid 20 (2001) 255–274.
[19] Z.H. Chen, Electro-magnetic control of cylinder wake. PhD dissertation, New Jersey Institute of Technology, Newark, NJ, 2001.
[20] H. Zhang, B.C. Fan, Z.H. Chen, B.M. Zhou, Suppression of flow separation around a circular cylinder by utilizing Lorentz force. China Ocean Engineering 22 (1) (2008) 87–95.
[21] J. Lim, J. Kim, A singular value analysis of boundary layer control. Physics of Fluids 16 (6) (2004) 1980–1988.
[22] M.D. Gunzburger, Perspectives in Flow Control and Optimization. SIAM, Philadelphia, 2003.
[23] F. Abergel, R. Teman, On some control problems in fluid mechanics. Theoretical and Computational Fluid Dynamics 1 (1990) 303–325.
[24] T.R. Bewley, P. Moin, R. Teman, DNS-based predictive control of turbulence: an optimal benchmark for feedback algorithms. Journal of Fluid Mechanics 447 (2001) 179–225.
[25] J. Soria, A. Ooi, M.S. Chong, Volume integrals of the Q_A–R_A invariants of the velocity gradient tensor in incompressible flows. Fluid Dynamics Research 19 (1997) 219–233.
[26] T.R. Bewley, Flow control: new challenges for a new renaissance. Progress in Aerospace Science 37 (2001) 21–58.